PCCP

High-throughput calculation for screening of Formamidinium Halide Perovskite for Solar Cells

Journal:	*Physical Chemistry Chemical Physics*
Manuscript ID	CP-ART-03-2024-000980.R1
Article Type:	Paper
Date Submitted by the Author:	12-Apr-2024

Complete List of Authors:	Tashiro, Tomoya; Hokkaido University, Department of Chemistry Suzuki, Hajime; Hokkaido University, Department of Chemistry Takahashi, Keisuke; Hokkaido University, Department of Chemistry

Journal Name

ARTICLE TYPE

Cite this: DOI: 10.1039/xxxxxxxxxx

High-throughput calculation for screening of Formamidinium Halide Perovskite for Solar Cells

Tomoya Tashiro[a], Hajime Suzuki[a], Keisuke Takahashi*[a]

Received Date
Accepted Date

DOI: 10.1039/xxxxxxxxxx

www.rsc.org/journalname

128 organic halide perovskites are systematically investigated using high throughput first principle calculations where Ge and Sn based materials are searched. The results revealed that all calculated materials exhibited exothermic reactions. Notably, a correlation between the heat of formation and X-site ions are identified. Six specific compounds, namely FA-Ge-I-I-I, FA-Sn-F-I-I, FA-Sn-Cl-I-I, FA-Sn-Br-Br-I, FA-Sn-Br-I-I, and FA-Sn-I-I-I where FA stands as formamidinium, are found to have a bandgap ranging from 1.0 to 2.0 eV, characterized by a direct bandgap in their band structure. Electronic structure analysis indicated that the CBM(Conduction band minimum) is influenced by the B-site p-orbital, while the VBM(Valence band maximum) is influenced by the X-site p-orbitals. This study underscores the capability of high throughput calculations to unveil hidden trends in perovskite materials, offering an effective approach for the exploration of promising perovskite materials.

1 Introduction

Since the first report on $CH_3NH_3PbX_3$ (X = Br and I) as a semiconductor sensitizer for dye-sensitized solar cells in 2009[1], organic–inorganic metal halide perovskite solar cells (PSCs) have drawn much attentions due to their high power conversion efficiency (PCE) and low production costs. The PCE of long-term durable solid-state perovskite solar cells first reported in 2012 was 9.7%, while a certified PCE of 25.7% was achieved in 2021[2,3]. Major improvement of PCE is progressed due to the development of formamidinium(FA)-based PSCs along the methylammonium-based PSCs[4–6]. This high photovoltaic performance is attributed to the high charge carrier mobility, high absorption coefficients, long diffusion lengths, and low exciton binding energy[7–11]. Materials with such perovskite crystal structures are of great interest in solar cells and optoelectronic applications, many of which are lead-halide perovskites(LHP). LHPs with the general formula of ABX_3 have the advantage that the performance of optoelectronic devices can be easily controlled by changing their composition[12]. In the semiconductor LHP, the charge of each site is +1 for the A-site, +2 for the B-site, and -1 for the X site, which can be replaced by ions of the same charge. For this reason, many studies have been conducted in recent years to replace the B-site with ions other than lead, which is highly toxic, but have yet to develop optoelectronic devices that are comparable to LHP[13,14]. There are several candidates for each site, such as MA, FA, and Cs^+ at the A-site, and Sn^{2+} and Ge^{2+} at the B-site, and some of the combinations have been experimentally synthesized and verified, but few methods have been established to understand the full picture and search for useful optoelectronic device materials[15,16]. In addition to these, each site can contain countless types of ions, and the number of combinations is enormous.

One large-scale screening technique in the materials space that can be challenging due to the large material synthesis to characterization where high-throughput (HTP) calculations can be an alternative screening technique[17–21]. Here, formamidinium(FA) based organic metal halide perovskite is explored using high throughput calculations. In particular, FA is chosen as a A site, Ge and Sn are chosen as B site, and, F, Cl, Br, and I are chosen as X site [22–24] where the bandgap of 1.4 eV is set as a target for solar cell applications[25].

2 Methods

High-throughput(HTP) calculation is implemented for searching perosvkite materials. Work flow of high throughput calculation is shown in Figure 1. First, atomic models for first principles calculations are constructed. Here, unit cell of cubic is used where the A-site containing formamidinium (FA), the B-site containing Ge or Sn, and one of the three X-sites containing either F, Cl, Br, or I. 128 different compositions of perovskite are constructed. An

[a] Department of Chemistry, Hokkaido University, North 10, West 8, Sapporo 060-0810, Japan
* email:tt.hokudai7613@eis.hokudai.ac.jp
* email:keisuke.takahashi@sci.hokudai.ac.jp

† Electronic Supplementary Information (ESI) available: [details of any supplementary information available should be included here]. See DOI: 10.1039/b000000x/

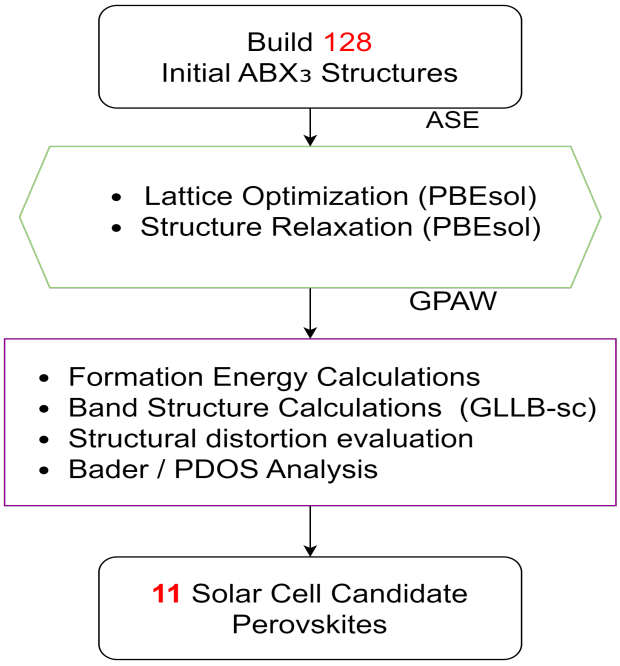

Fig. 1 Workflow of proposed high throughput calculations.

example of the initial structure is shown in Figure 2. Note that X-site can contain three different anions (e.g. FA-Ge-Cl-Br-I). All compositions with rearranged X-sites, such as FA-Ge-F-I-I, FA-Ge-I-F-I, and FA-Ge-I-I-F, are distinguished in the calculation due to the structure of FA. It must be also noted that conformation and coordinates of FA in initial structure is fixed, therefore, the conformation and coordinates of FA might not be the ground states. The initial unit cell is 5.66Å × 5.66Å × 5.66Å.

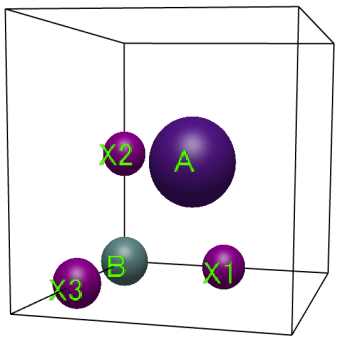

Fig. 2 The basic structure of formamidinium halide perovskite where A, B, and X(1,2,3) are denoted at each site. FA in the A-site, Ge or Sn in the B-site, and F, Cl, Br, or I in each X-site.

Next, first-principles calculations are performed where the grid-based projector-augmented-wave (GPAW)[26] method with the finite difference mode is implemented. In GPAW, the exchange–correlation of Perdew-Burke-Ernzerhof revised for solids (PBEsol[27]) is applied for structural relaxation calculation. Grid space for structure optimization is set to 0.18 Å. Special k points of the Brillouin zone sampling (4 × 4 × 4) are used within periodic boundary conditions in the x, y and z axes[28]. Then, analysis of the formation energy and electronic structure is performed. The formation energy is calculated based on eq 1. E_A , E_B and E_{X_i} are reference energy of pristine bulk materials/molecules. Note that negative(positive) sign indicates an exothermic(endothermic) reaction.

$$E_{ABX_3} = \frac{E_{all} - (E_A + E_B + \sum_{i=1,2,3} E_{X_i})}{N} \quad (1)$$

Distortion of the crystal structure is evaluated using the deviation of X-site ions from ideal atomic coordinates. The X-site ions in cubic perovskite ideally reside at the midpoints of the edges of the lattice. Therefore, the lattice distortion (%) is defined by dividing the distance of the X-site ion from this point in the optimized structure by the lattice constant.

In the analysis of electronic structure, the band structure is first calculated. Exchange correlation of GLLB-SC is used for band structure calculation. Grid space is set to 0.22 Å for band gap calculation. K point path of [Γ, R, M, X] is used. In candidate materials with suitable band gaps for solar cells, projected density of states (PDOS) and bader analysis is also implemented[29, 30].

3 Results and discussion

High throughput calculations are performed for all 128 cases. Formation energy of each compositions of perovskites are visualized in Figure 3. Note that data for FA-Sn-F-F-F, FA-Sn-F-F-Cl and FA-Sn-F-F-Br are not able to be acquired due to the convergence errors during structural optimization. Figure 3 demonstrates that all calculated perovskite have exothermic formation energy, thus all of them are thermodynamically stable. The compositions containing F in the X-site tend to be highly distorted from the cubic crystal (e.g. Figure 4). The lattice distortion of FA-Ge-F-F-F shown in Figure 4(a) is 27%, which is larger than one in FA-Sn-I-I-I as shown in Figure 4(b), where the lattice distortion is 4.8%. The gray color in Figure 3 indicates a structure with lattice distortion greater than 15 %. These are distorted and collapsed structures. The 15% threshold is set because, as shown in Figure 5, there is a gap in the frequency distribution when the lattice distortion is greater than 15%.

Figure 6 shows the pairwise correlation values for each property of perovskite. Pairwise correation demonstrate the linear correation where positive and negative correlation represent proportional and inverse proportional relation, respectively. As can be seen in Figure 6, there is a strong negative correlation between the lattice distortion(LD) and Formation energy(E_{ABX_3}). X site ions except F has a positive correlation with the heat of formation. F has a negative correlation with the heat of formation and those are resulted by large structural distortion. There is also a positive correlation between lattice distortion and band gap values. In particular, Figure 7 shows a plot of band gap versus lattice distortion. Figure 7 shows that most of the compositions with lattice distortion above 15% have band gaps above 3.0 eV, which is well away from the solar cell target.

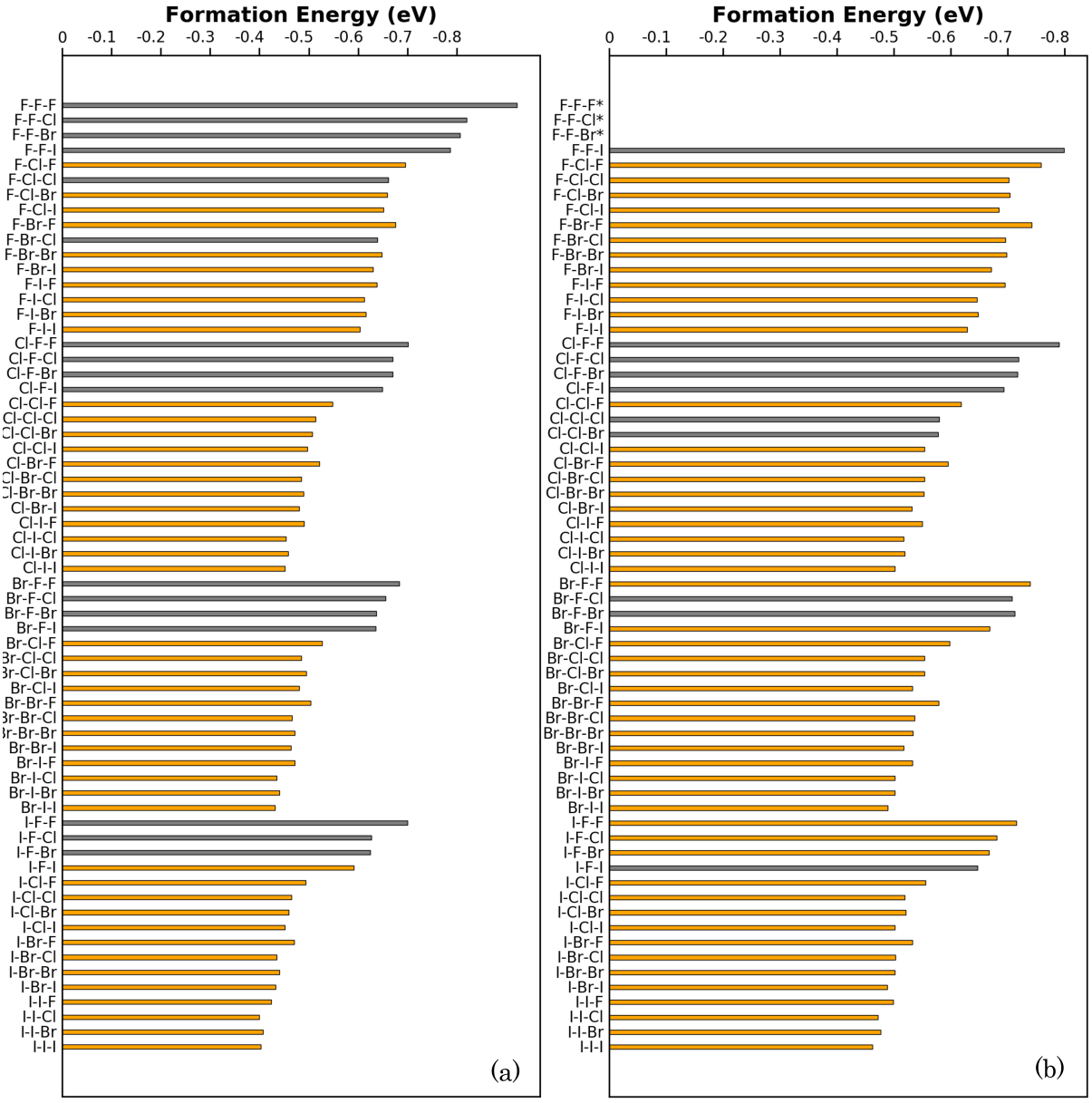

Fig. 3 (a)Formation energy of Ge-Based Compositions and (b)Formation energy of Sn-Based Compositions Compositions with gray bars indicates a structure with lattice distortion greater than 15 %. All calculated perovskites have exothermic formation energies and are therefore thermodynamically stable. Composition with $*$ has no data due to convergence errors.

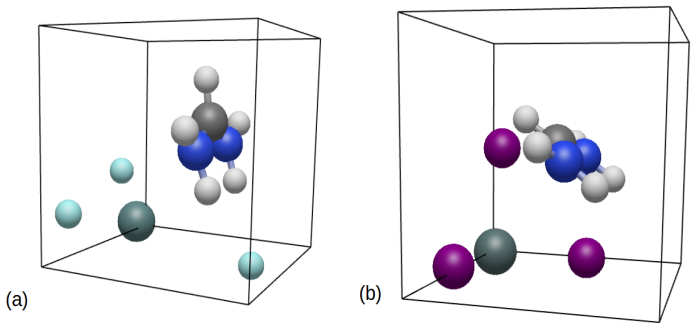

Fig. 4 Distruped and undistruped structure.(a)Crystal structure of disrupted FA-Ge-F-F-F. Lattice distortion: 27%. Color code:Gray;Ge, Light Blue;F. (b) Undisrupted crystal structure FA-Sn-I-I-I. Lattice distortion: 4.8%. Color code:Gray;Sn, Purple;I.

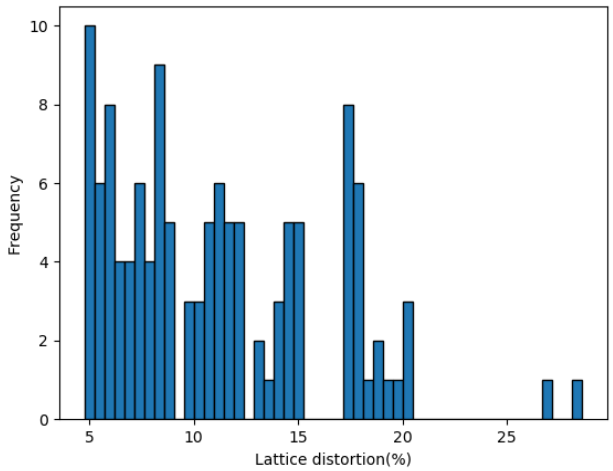

Fig. 5 Frequency distribution of the lattice distortion where the lattice distortion is the maximum distance that X-site ions have migrated from the ideal coordinates in the optimized structure divided by the lattice constant. There is a frequency gap at 15% lattice distortion, which is used as a criterion for whether the structure is collapsing or not.

Table 1 Charge transfer of B and X site atoms for selected perosvkites.

ABX_3	B-site Charge	X_1-X_2-X_3-site Charge		
Ge-based				
FA-Ge-F-F-F	+1.57	-0.80	-0.78	-0.91
FA-Ge-F-F-I	+1.35	-0.81	-0.83	-0.64
FA-Ge-F-I-I	+1.14	-0.79	-0.57	-0.62
FA-Ge-I-I-I	+0.86	-0.55	-0.54	-0.60
Sn-based				
FA-Sn-F-F-I	+1.40	-0.83	-0.83	-0.67
FA-Sn-F-I-I	+1.18	-0.78	-0.63	-0.63
FA-Sn-I-I-I	+0.98	-0.61	-0.61	-0.60

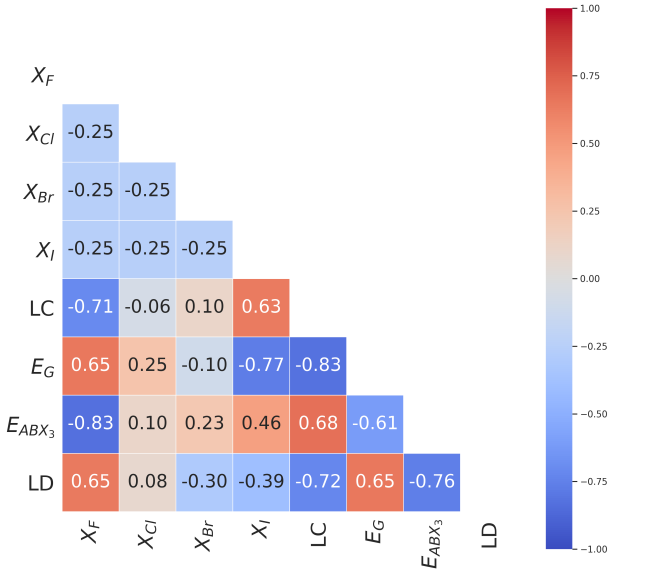

Fig. 6 Pairwise correation of each property of perovskite.. XF,XCl,XBr,XI: Fraction of each halogen in X-site. LC: Lattice constant. E_G: Bandgap(E_{KS+DXC}). E_{ABX_3}: Formation energy. LD: Lattice distortion.

The electronic structures of compositions with high (e.g. FA-Ge-F-F-F) and low (e.g. FA-Ge-I-I-I) heat of formation are investigated. The charge transfer of the B-site atoms are listed in Table 1. In FA-Ge-F-F-F, F is negatively charged by 0.80, 0.78, and 0.91 electrons, respectively, while Ge is positively charged by 1.57 electrons. On the other hand, in FA-Ge-I-I-I, I is negatively charged by 0.55, 0.54, and 0.60 electrons, while Ge is positively charged by 0.86 electrons Bader analysis indicates that the compositions with F in the X-sites have more positively charged B-site atoms than compositions with I. Thus, it is suggested that F forms stronger ionic bonds with the B-site atoms, thereby inducing structural distortions.

Here, two type of bandgap is calculated named E_{KS} and E_{KS+DXC}. E_{KS} is bandgap calculated by PBE exchange correlation while E_{KS+DXC} is calculated by exchange correlation of GLLB-sc[31,32]. In particular, E_{KS+DXC} is the fundamental band gap (eV) of GLLB-sc (DXC is a differential discontinuity)[31,32]. The discrepancy between the correction by DXC and the actual experimental values varies from system to system. Table 2 shows calculated and experimental band gap values for some compositions. Cal-

Table 2 Calculated (E_{KS}, E_{KS+DXC}) and experimental band gaps of $FAGeBr_3$, $FAGeI_3$, $FASnBr_3$ and $FASnI_3$

Composition	E_{KS} [eV]	E_{KS+DXC} [eV]	Exp.
FA-Ge-Br-Br-Br	2.26	3.23	3.13[33]
FA-Sn-Br-Br-Br	1.83	2.62	2.37[34]
FA-Ge-I-I-I	1.30	1.87	2.20[35]
FA-Sn-I-I-I	0.71	1.01	1.44[36]

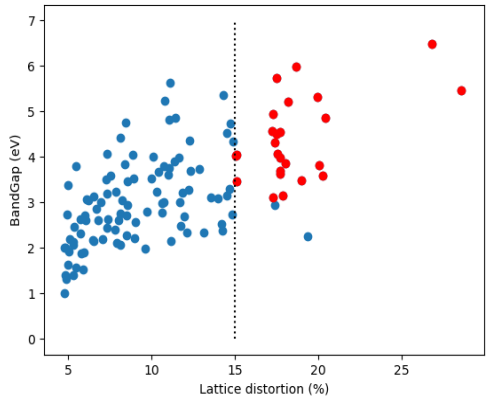

Fig. 7 Bandgap against lattice distortion is visualized. The vertical dotted line indicates an lattice distortion value of 15%, and the red dots indicate compositions with a lattice distortion greater than 15% and a band gap greater than 3.0 eV.

Table 3 Composition, LC(lattice constants), Formation Energy(E_{ABX_3}) and Band gap(E_{KS+DXC}) of 11 candidated perovskites .

ABX_3	LC[Å]	E_{ABX_3} [eV]	E_{KS+DXC} [eV]
FA-Ge-I-I-I	6.20	-0.403	1.87
FA-Sn-F-I-I	6.25	-0.628	1.98
FA-Sn-Cl-I-I	6.25	-0.502	1.57
FA-Sn-Br-Br-I	6.20	-0.517	1.91
FA-Sn-Br-I-I	6.25	-0.489	1.40
FA-Sn-I-Cl-I	6.25	-0.502	1.52
FA-Sn-I-Br-Br	6.25	-0.502	1.93
FA-Sn-I-Br-I	6.25	-0.488	1.41
FA-Sn-I-I-Cl	6.25	-0.472	1.64
FA-Sn-I-I-Br	6.25	-0.476	1.32
FA-Sn-I-I-I	6.30	-0.463	1.01

culated bandgap with E_{KS+DXC} have a good agreement with experimental bandgap[33–36]. Therefore, E_{KS+DXC} is chosen for calculating bandgap.Band gap of each compositions of perovskites are visualized in Figure 8. One can see that, the larger the sum of the electronegativity of the X-site atoms, the wider the band gap (e.g. FAGeF-F-F:6.50 eV, FAGeI-I-I:1.87 eV). The 11 compositions with bandgaps of 1.0∼2.0 (eV) are listed in Table 3. The compositions such as FA-Sn-Cl-I-I, FA-Sn-I-Cl-I, and FA-Sn-I-I-Cl are similar to each other. Therefore, considering them as equivalent compositions in this work, the candidate compositions can be described as $FAGeI_3$, $FASnI_2F$, $FASnI_2Cl$, $FASnIBr_2$, $FASnI_2Br$, and $FASnI_3$. Note that all compositions contain I. This is confirmed by the strong negative correlation of the number of X-site I ions against the bandgap shown in Figure 6, indicating that the presence of I might play an important role for controlling band gap. All of these compositions are based on partial substitution of $FAGeI_3$ and $FASnI_3$ with other halogens. In particular, Br^- doped $FASnI_3$ has been studied previously as a solar cell, and the results are in good agreement with the calculations[37–40].

Projected density of states (PDOS) are investigated to further understanding of the band structure as shown in Figure 9. In particular, materials that has band gap range of 1.0-2.0 eV are investigated. One can see that, the B-site p-orbital is dominant for CBM(Conduction band minimum) and the X-site p-orbitals are dominant for VBM(Valence band maximum). These PDOS indicate that the energy level of the p orbital of I in the VBM is higher than the p orbital of other halogens. Therefore, X-site atoms with higher energy levels in the VBM, such as I, are important to achieve a narrower band gap. Band structure are also summarized in Figure 10. Band structure analysis indicates that all candidate compositions are semiconductors and have direct band gap. The lattice distortion for each composition is shown in Figure S3.

4 Conclusion

In summary, 128 Ge,Sn based organic halide perovskites are investigated by high throughput calculations. All of calculated materials have exothermic reaction. Calculations unveil that there are some correlation between the heat of formation and X site ions. In particular, FA-Ge-I-I-I, FA-Sn-F-I-I, FA-Sn-Cl-I-I, FA-Sn-Br-Br-I, FA-Sn-Br-I-I, and FA-Sn-I-I-I have bandgap between 1.0 - 2.0 eV where band structure shows these have direct bandgap. Electronic structures demonstrate that B-site p-orbital is responsible for CBM and the X-site p-orbitals are responsible for VBM. Thus, high throughput calculation can unveil the hidden trends in perovskite materials and effectively search the perovskite materials.

5 Supporting Information

Calcualted all data is included as Supporting Information

6 Acknowledgement

This work is funded by Japan Science and Technology Agency(JST) CREST Grant Number JPMJCR17P2, ERATO grant number JPMJER1903,JST Mirai Program Grant Number JPMJMI22G4, JSPS KAKENHI Grant-in-Aid for Scientific Research (B) Grant Number JP23H01762.

Notes and references

1 Akihiro Kojima, Kenjiro Teshima, Yasuo Shirai, and Tsutomu Miyasaka, Organometal halide perovskites as visible-light sensitizers for photovoltaic cells, *Journal of the american chemical society*, 2009, **131**(17), 6050–6051.

2 Hui-Seon Kim, Chang-Ryul Lee, Jeong-Hyeok Im, Ki-Beom Lee, Thomas Moehl, Arianna Marchioro, Soo-Jin Moon, Robin Humphry-Baker, Jun-Ho Yum, Jacques E Moser, et al, Lead iodide perovskite sensitized all-solid-state submicron thin film mesoscopic solar cell with efficiency exceeding 9%, *Scientific reports*, 2012, **2**(1), 591.

3 Hanul Min, Do Yoon Lee, Junu Kim, Gwisu Kim, Kyoung Su Lee, Jongbeom Kim, Min Jae Paik, Young Ki Kim, Kwang S Kim, Min Gyu Kim, et al, Perovskite solar cells with atomically coherent interlayers on sno2 electrodes, *Nature*, 2021, **598**(7881), 444-450.

4 Dongqin Bi, Wolfgang Tress, M Ibrahim Dar, Peng Gao, Jingshan Luo, Clémentine Renevier, Kurt Schenk, Antonio Abate, Fabrizio Giordano, Juan-Pablo Correa Baena, et al, Efficient luminescent solar cells based on tailored mixed-cation perovskites, *Science advances*, 2016, **2**(1), e1501170.

5 Michael Saliba, Taisuke Matsui, Konrad Domanski, Ji-Youn Seo, Amita Ummadisingu, Shaik M Zakeeruddin, Juan-Pablo Correa-Baena, Wolfgang R Tress, Antonio Abate, Anders Hagfeldt, et al, Incorporation of rubidium cations into perovskite solar cells improves photovoltaic performance, *Science*, 2016, **354**(6309), 206-209.

6 Changlei Wang, Dewei Zhao, Yue Yu, Niraj Shrestha, Corey R Grice, Weiqiang Liao, Alexander J Cimaroli, Jing Chen, Randy J Ellingson, Xingzhong Zhao, et al, Compositional and morphological engineering of mixed cation perovskite films for highly efficient planar and flexible solar cells with reduced hysteresis, *Nano Energy*, 2017, **35**, 223-232.

7 Guichuan Xing, Nripan Mathews, Shuangyong Sun, Swee Sien Lim, Yeng Ming Lam, Michael Grätzel, Subodh Mhaisalkar, and Tze Chien Sum, Long-range balanced electron-and hole-transport lengths in organic-inorganic ch3nh3pbi3, *Science*, 2013, **342**(6156), 344-347.

8 Feng Hao, Constantinos C Stoumpos, Duyen Hanh Cao, Robert PH Chang, and Mercouri G Kanatzidis, Lead-free solid-state organic–inorganic halide perovskite solar cells, *Nature photonics*, 2014, **8**(6), 489-494.

9 Samuel D Stranks, Giles E Eperon, Giulia Grancini, Christopher Menelaou, Marcelo JP Alcocer, Tomas Leijtens, Laura M Herz, Annamaria Petrozza, and Henry J Snaith, Electron-hole diffusion lengths exceeding 1 micrometer in an organometal trihalide perovskite absorber, *Science*, 2013, **342**(6156), 341-344.

10 Michael M Lee, Joël Teuscher, Tsutomu Miyasaka, Takurou N Murakami, and Henry J Snaith, Efficient hybrid solar cells based on meso-superstructured organometal halide perovskites, *science*, 2012, **338**(6107), 643-647.

11 Wenbin Deng, Faming Li, Jianyang Li, Ming Wang, Yuchao Hu, and Mingzhen Liu, Anti-solvent free fabrication of fa-based perovskite at low temperature towards to high performance flexible perovskite solar cells, *Nano Energy*, 2020, **70**, 104505.

12 Bright Walker, Gi-Hwan Kim, and Jin Young Kim, Pseudohalides in lead-based perovskite semiconductors, *Advanced Materials*, 2019, **31**(20), 1807029.

13 Maria Konstantakou and Thomas Stergiopoulos, A critical review on tin halide perovskite solar cells, *Journal of Materials Chemistry A*, 2017, **5**(23), 11518-11549.

14 Indira Kopacic, Bastian Friesenbichler, Sebastian F Hoefler, Birgit Kunert, Harald Plank, Thomas Rath, and Gregor Trimmel, Enhanced performance of germanium halide perovskite solar cells through compositional engineering, *ACS Applied Energy Materials*, 2018, **1**(2), 343-347.

15 Prashant V Kamat, Juan Bisquert, and Jillian Buriak, Lead-free perovskite solar cells, *ACS Energy Letters*, 2017, **2**(4), 904-905.

16 Christopher N Savory, Aron Walsh, and David O Scanlon, Can pb-free halide double perovskites support high-efficiency solar cells?, *ACS energy letters*, 2016, **1**(5), 949-955.

17 Daniele Torelli, Hadeel Moustafa, Karsten W Jacobsen, and Thomas Olsen, High-throughput computational screening for two-dimensional magnetic materials based on experimental databases of three-dimensional compounds, *npj Computational Materials*, 2020, **6**(1), 158.

18 Ankit Jain, Oleksandr Voznyy, and Edward H Sargent, High-throughput screening of lead-free perovskite-like materials for optoelectronic applications, *The Journal of Physical Chemistry C*, 2017, **121**(13), 7183-7187.

19 Xinfeng Diao, Yongxin Diao, Yanlin Tang, Gangling Zhao, Qinzhong Gu, Yu Xie, Yebai Shi, Ping Zhu, and Liang Zhang, High-throughput screening of stable and efficient double inorganic halide perovskite materials by dft, *Scientific Reports*, 2022, **12**(1), 12633.

20 Takahito Nakajima and Keisuke Sawada, Discovery of pb-free perovskite solar cells via high-throughput simulation on the k computer, *The journal of physical chemistry letters*, 2017, **8**(19), 4826-4831.

21 Keisuke Takahashi, Lauren Takahashi, Son Dinh Le, Takaaki Kinoshita, Shun Nishimura, and Junya Ohyama, Synthesis of heterogeneous catalysts in catalyst informatics to bridge experiment and high-throughput calculation, *Journal of the American Chemical Society*, 2022, **144**(34), 15735-15744.

22 Haizhou Lu, Yuhang Liu, Paramvir Ahlawat, Aditya Mishra, Wolfgang R Tress, Felix T Eickemeyer, Yingguo Yang, Fan Fu, Zaiwei Wang, Claudia E Avalos, et al, Vapor-assisted deposition of highly efficient, stable black-phase fapbi3 perovskite solar cells, *Science*, 2020, **370**(6512), eabb8985.

23 Nacereddine Lakhdar and Abdelkader Hima, Electron transport material effect on performance of perovskite solar cells based on ch3nh3gei3, *Optical Materials*, 2020, **99**, 109517.

24 Shuyan Shao, Jian Liu, Giuseppe Portale, Hong-Hua Fang, Graeme R Blake, Gert H ten Brink, L Jan Anton Koster, and Maria Antonietta Loi, Highly reproducible sn-based hybrid perovskite solar cells with 9% efficiency, *Advanced Energy Materials*, 2018, **8**(4), 1702019.

25 Bruno Ehrler, Esther Alarcón-Lladó, Stefan W Tabernig, Tom Veeken, Erik C Garnett, and Albert Polman, Photovoltaics reaching for the shockley–queisser limit, 2020, 3029-3033.

26 Jens Jørgen Mortensen, Lars Bruno Hansen, and Karsten Wedel Jacobsen, Real-space grid implementation of the projector augmented wave method, *Physical review B*, 2005, **71**(3), 035109.

27 John P Perdew, Adrienn Ruzsinszky, Gábor I Csonka, Oleg A Vydrov, Gustavo E Scuseria, Lucian A Constantin, Xiaolan Zhou, and Kieron Burke, Restoring the density-gradient expansion for exchange in solids and surfaces, *Physical review*

letters, 2008, **100**(13), 136406.

28 Hendrik J Monkhorst and James D Pack, Special points for brillouin-zone integrations, *Physical review B*, 1976, **13**(12), 5188.

29 Graeme Henkelman, Andri Arnaldsson, and Hannes Jónsson, A fast and robust algorithm for bader decomposition of charge density, *Computational Materials Science*, 2006, **36**(3), 354–360.

30 W Tang, E Sanville, and G Henkelman, A grid-based bader analysis algorithm without lattice bias, *Journal of Physics: Condensed Matter*, 2009, **21**(8), 084204.

31 Maria KY Chan and Gerbrand Ceder, Efficient band gap prediction for solids, *Physical review letters*, 2010, **105**(19), 196403.

32 Hajime Suzuki, Itsuki Miyazato, Tanveer Hussain, Fatih Ersan, Satoshi Maeda, and Keisuke Takahashi, Designing two-dimensional dodecagonal boron nitride, *CrystEngComm*, 2022, **24**(3), 471-474.

33 Yang Liu, Ya-Ping Gong, Shining Geng, Mei-Ling Feng, Despoina Manidaki, Zeyu Deng, Constantinos C Stoumpos, Pieremanuele Canepa, Zewen Xiao, Wei-Xiong Zhang, et al, Hybrid germanium bromide perovskites with tunable second harmonic generation, *Angewandte Chemie International Edition*, 2022, **61**(43), e202208875.

34 Ambra Pisanu, Arup Mahata, Edoardo Mosconi, Maddalena Patrini, Paolo Quadrelli, Chiara Milanese, Filippo De Angelis, Lorenzo Malavasi, et al, Exploring the limits of three-dimensional perovskites: The case of fapb1–xsnxbr3, *ACS ENERGY LETTERS*, 2018, **3**(6), 1353-1359.

35 Constantinos C Stoumpos, Laszlo Frazer, Daniel J Clark, Yong Soo Kim, Sonny H Rhim, Arthur J Freeman, John B Ketterson, Joon I Jang, and Mercouri G Kanatzidis, Hybrid germanium iodide perovskite semiconductors: active lone pairs, structural distortions, direct and indirect energy gaps, and strong nonlinear optical properties, *Journal of the American Chemical Society*, 2015, **137**(21), 6804-6819.

36 Rebecca L Milot, Giles E Eperon, Thomas Green, Henry J Snaith, Michael B Johnston, and Laura M Herz, Radiative monomolecular recombination boosts amplified spontaneous emission in hc (nh2) 2sni3 perovskite films, *The journal of physical chemistry letters*, 2016, **7**(20), 4178-4184.

37 Meng Zhang, Miaoqiang Lyu, Jung-Ho Yun, Mahir Noori, Xiaojing Zhou, Nathan A Cooling, Qiong Wang, Hua Yu, Paul C Dastoor, and Lianzhou Wang, Low-temperature processed solar cells with formamidinium tin halide perovskite/fullerene heterojunctions, *Nano Research*, 2016, **9**, 1570-1577.

38 Seon Joo Lee, Seong Sik Shin, Jino Im, Tae Kyu Ahn, Jun Hong Noh, Nam Joong Jeon, Sang Il Seok, and Jangwon Seo, Reducing carrier density in formamidinium tin perovskites and its beneficial effects on stability and efficiency of perovskite solar cells, *ACS Energy Letters*, 2017, **3**(1), 46-53.

39 Chengbo Wang, Yuting Zhang, Feidan Gu, Ziran Zhao, Haisheng Li, Hong Jiang, Zuqiang Bian, and Zhiwei Liu, Illumination durability and high-efficiency sn-based perovskite solar cell under coordinated control of phenylhydrazine and halogen ions, *Matter*, 2021, **4**(2), 709-721.

40 Mengmeng Chen, Muhammad Akmal Kamarudin, Ajay K Baranwal, Gaurav Kapil, Teresa S Ripolles, Kohei Nishimura, Daisuke Hirotani, Shahrir Razey Sahamir, Zheng Zhang, Chao Ding, et al, High-efficiency lead-free wide band gap perovskite solar cells via guanidinium bromide incorporation, *ACS Applied Energy Materials*, 2021, **4**(6), 5615-5624.

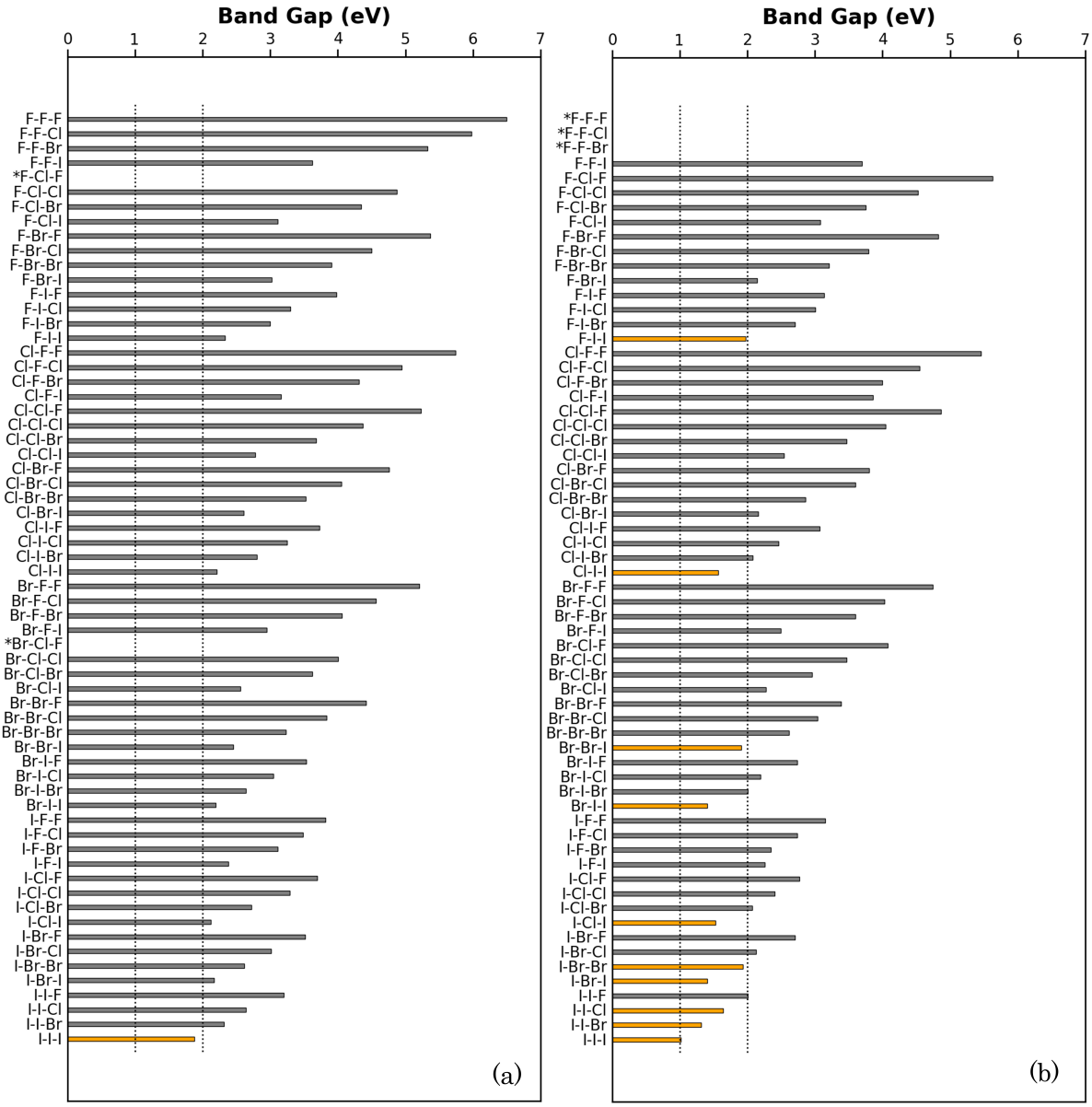

Fig. 8 (a)Band Gap(E_{KS+DXC}) of Ge-Based Compositions (b)Band Gap(E_{KS+DXC}) of Sn-Based Compositions. E_{KS+DXC}:Fundamental band gap of GLLB-sc (eV) are visualized where DXC is derivative discontinuity. The dotted lines are at 1.0 eV and 2.0 eV, and the composition of the orange bars indicates that the band gap lies between them. Composition with $*$ has no data due to convergence errors.

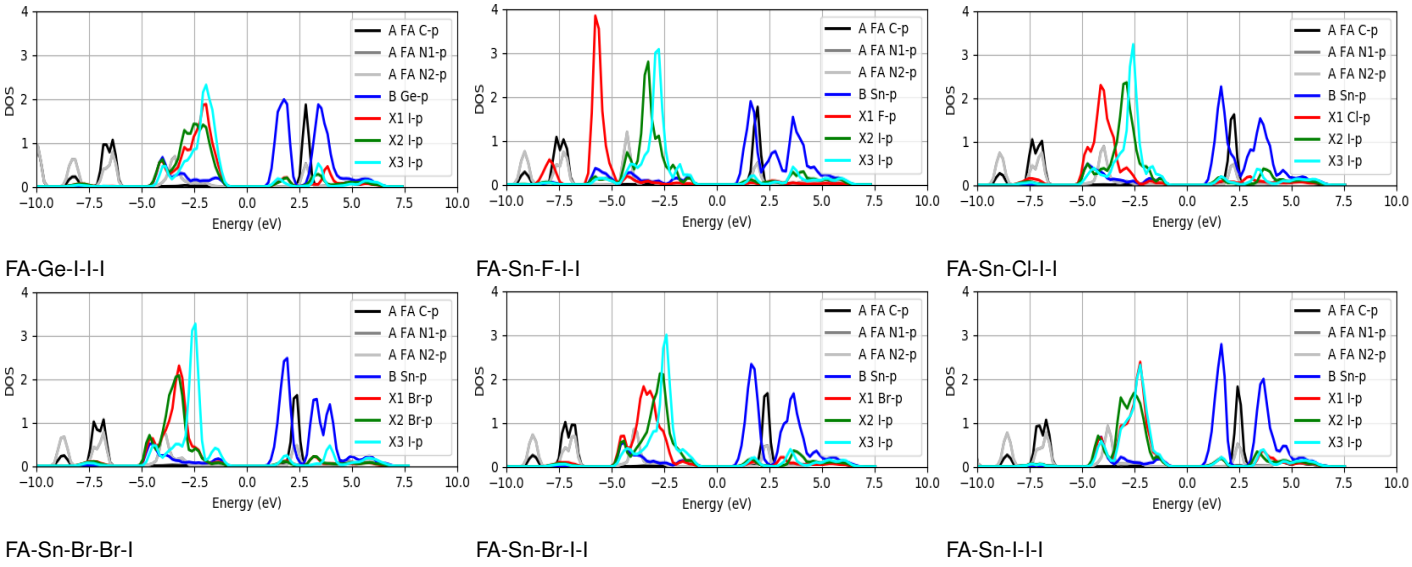

Fig. 9 Projected density of states (PDOS) of 6 representative candidate compositions. 6 compositions are selected as representative candidates from 11 candidate compositions by rearranging the compositions that have the same X-site composition. The C and two N p-orbital of FA in the A-site are shown in black and gray, the Ge and S p-orbital in the B-site in blue, and the p-orbital of each ion in the X-site in red, green, and yellow.

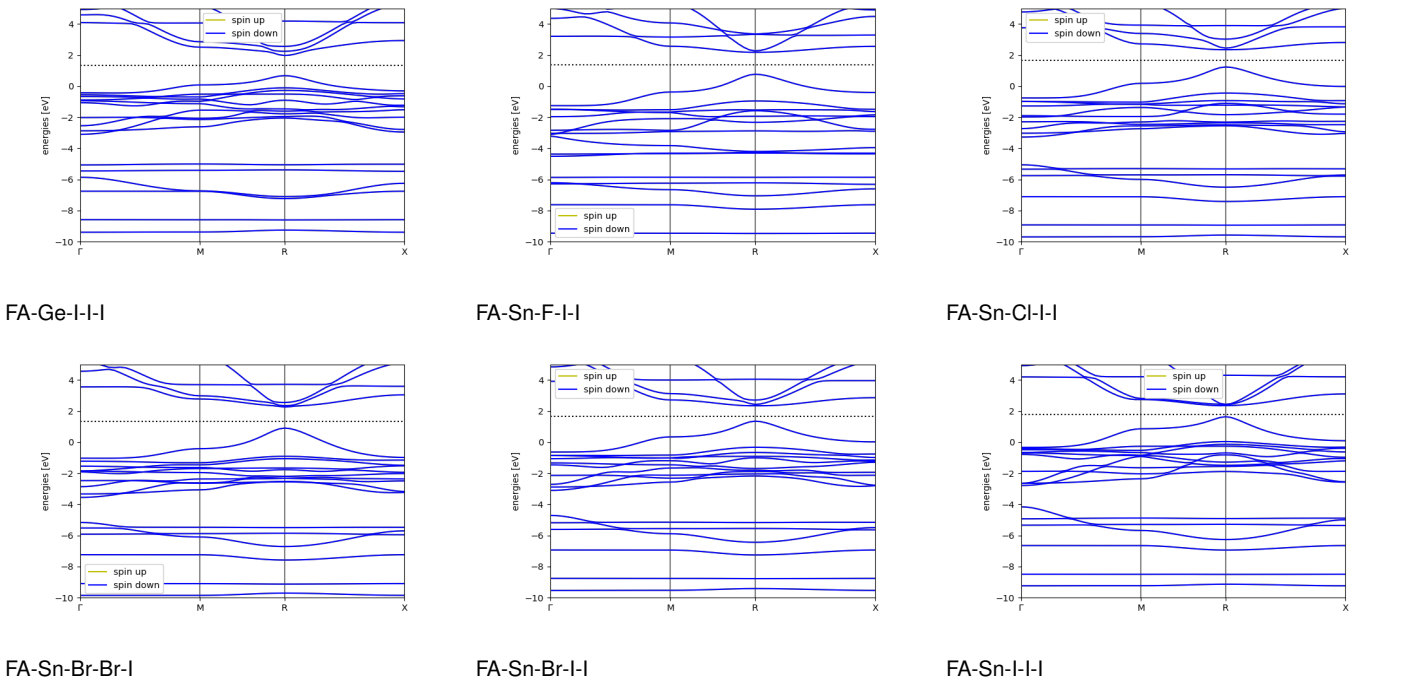

Fig. 10 E_{KS+DXC}(GLLB-sc) band structure for compositions with band gap from 1.0∼2.0 eV. 6 compositions are selected as representative candidates from 11 candidate compositions by rearranging the compositions that have the same X-site composition.